Biochimica et Biophysica Acta 1832 (2013) 20–28

Contents lists available at SciVerse ScienceDirect

Biochimica et Biophysica Acta

journal homepage: www.elsevier.com/locate/bbadis

Binding of methylene blue to a surface cleft inhibits the oligomerization and fibrillization of prion protein

Paola Cavaliere [a,b,1], Joan Torrent [c], Stephanie Prigent [c], Vincenzo Granata [b], Kris Pauwels [d,2], Annalisa Pastore [d], Human Rezaei [c,*], Adriana Zagari [a,b,**]

[a] Dipartimento delle Scienze Biologiche, Università degli Studi di Napoli "Federico II", Napoli, Italy
[b] CEINGE, Biotecnologie Avanzate S.c.a r.l., Napoli, Italy
[c] Institut National de la Recherche Agronomique (INRA), Virologie et Immunologie Moléculaires, Equipe Biologie Physico-chimique des Prions, Jouy-en-Josas, France
[d] MRC National Institute for Medical Research, The Ridgeway, London NW7 1AA, UK

ARTICLE INFO

Article history:
Received 19 July 2012
Received in revised form 14 September 2012
Accepted 17 September 2012
Available online 25 September 2012

Keywords:
Amyloidogenic protein
PrP oligomer
PrP fiber
Anti-prion agent
Neurodegenerative disease

ABSTRACT

Neurodegenerative protein misfolding diseases, including prionopathies, share the common feature of accumulating specific misfolded proteins, with a molecular mechanism closely related. Misfolded prion protein (PrP) generates soluble oligomers that, in turn, aggregate into amyloid fibers. Preventing the formation of these entities, crucially associated with the neurotoxic and/or infectious properties of the resulting abnormal PrP, represents an attractive therapeutic strategy to ameliorate prionopathies. We focused our attention into methylene blue (MB), a well-characterized drug, which is under study against Alzheimer's disease and other neurodegenerative disorders. Here, we have undertaken an in vitro study on the effects of MB on oligomerization and fibrillization of human, ovine and murine PrP. We demonstrated that MB affects the kinetics of PrP oligomerization and reduces the amount of oligomer of about 30%, in a pH-dependent manner, by using SLS and DSC methodologies. Moreover, TEM images showed that MB completely suppresses fiber formation at a PrP:MB molar ratio of 1:2. Finally, NMR revealed a direct interaction between PrP and MB, which was mapped on a surface cleft including a fibrillogenic region of the protein. Our results allowed to surmise a mechanism of action in which the MB binding to PrP surface markedly interferes with the pathway towards oligomers and fibres. Therefore MB could be considered as a general anti-aggregation compound, acting against proteinopathies.

1. Introduction

Neurodegenerative disorders such as Alzheimer's (AD), Parkinson's and Huntington diseases, frontotemporal dementia and prion diseases are included in the general family of protein misfolding pathologies. These diseases show substantial overlap in their pathologic mechanisms [1,2], with their main common characteristic being oligomer formation followed by fibrillar arrangement and deposition of misfolded proteins in the brain [3,4].

In particular, prion diseases are a family of rare but all fatal pathologies, which affect humans, e.g. the Creutzfeldt–Jakob disease, and various animal species, e.g. scrapie in sheep and goat, and bovine spongiform encephalopathies in cattle. It is commonly accepted that these diseases are caused by a conformational change of the cellular prion protein (PrP^C), which is rich in α-helix, to its β-sheet-rich insoluble conformer, called scrapie PrP (PrP^{Sc}) [5]. How this conformational transition occurs is not yet clearly elucidated, despite the plethora of studies [5–7]. All proposed mechanisms to describe the conversion of PrP^C into PrP^{Sc} suggest a multi-step process including an oligomerization/polymerization step [7,8]. Based on the assumption that one or more of the different conformational PrP states involved (i.e. oligomers, proto-fibrils, amyloid fibrils) correspond to the infectious and/or toxic entity, various approaches aimed at targeting such abnormal species are currently explored for therapeutic interventions.

Treating prion diseases remains a challenge for the scientific and medical community. Although a large number of anti-prion agents have been identified, none represents an efficient cure. For pragmatic reasons, and since the basic molecular mechanisms in protein misfolding disorders are closely related, it seems reasonable to surmise that some compounds, with anti-aggregation potency in various

Abbreviations: PrP, prion protein; MB, methylene blue; wt-OvPrP, ovine recombinant wild-type full-length PrP (23–234); ΔOvPrP, ovine recombinant truncated PrP (103–234); MoPrP, murine recombinant full-length PrP (23–231); wt-HuPrP, wild-type human recombinant full-length PrP (23–231); AD, Alzheimer's disease

* Corresponding author.
** Correspondence to: Dipartimento delle Scienze Biologiche, Università degli Studi di Napoli "Federico II", Napoli, Italy. Tel.: +39 081 3737913; fax: +39 081 3737808.
E-mail addresses: human.rezaei@jouy.inra.fr (H. Rezaei), adriana.zagari@unina.it (A. Zagari).
[1] Present address: Unité de Génétique Moléculaire, Institut Pasteur, Paris Cedex 15, France.
[2] Present address: VIB Department of Structural Biology, Vrije Universiteit Brussel, Brussel, Belgium.

0925-4439/$ – see front matter © 2012 Elsevier B.V. All rights reserved.
http://dx.doi.org/10.1016/j.bbadis.2012.09.005

model systems of protein misfolding and disease, might be also effective for prion diseases. Accordingly, we addressed our quest for new anti-prion agents to compounds that are well characterized with respect to their drug-like qualities. We focused on methylene blue (MB) which has been commonly used for the treatment of several medical conditions for at least 120 years [9] and currently being tested in phase II clinical trials in AD [10].

MB is a water-soluble dye, belonging to the phenothiazine class. This compound is approved by the Food and Drug Administration for oral or i.v. administration for several pathologies. From a toxicological point of view, MB is known to be scarcely toxic [10] and more important, MB is able to pass the blood–brain barrier [11,12]; hence, it is suitable to reach neuronal targets.

MB has recently attracted increasing attention, because it has been shown to slow down the progression of the AD patients with a net improvement of cognitive function [10]. Nevertheless, its mechanism of action remains unclear. At a molecular level, MB was found to interfere, in vitro, with the aggregation of the $A\beta_{42}$ [13], $A\beta_{40}$ peptides and tau proteins [14]. In addition, MB is able to antagonize other amyloidogenic proteins; indeed, MB can modulate the polyglutamine degradation, in a manner dependent on hsp70/hsp90 chaperone machinery [15], and impairs the deposition of the TAR DNA-binding protein (TDP-43) in a cell culture model over-expressing a TDP-43 variant [16].

Although these findings support the notion that MB displays anti-aggregating properties, the possibility of an interaction between PrP and MB has not yet been explored. An important study focused on phenothiazine structure–activity relationships and conducted in neuroblastoma ScN2a prion infected cells showed that MB was cytotoxic for ScN2a cells and not able to inhibit the PrP^{Sc} formation [17]. However, its action could not be reliably examined because of its toxicity toward these cells. On the other hand, in a recent study, red cells suspended in MB treated plasma were prepared for neonatal exchange transfusion [18].

In this scenario, the scarce knowledge of MB action on prion protein, with respect to other amyloidogenic proteins, prompted us to study the effects of this compound on the PrP aggregation process, by using an ensemble of biophysical methodologies. We report a direct interaction between MB and PrP, involving mainly the C-terminus of helix H2 and a small region around helix H1, that were shown to possess high propensity to aggregation [19]. By dissecting the action of MB along the polymerization reaction from monomers to fibrils, we demonstrated the effectiveness of this compound to antagonize both PrP oligomerization and fibrillization, by slowing down the formation of PrP oligomers, reducing their amount and completely suppressing the formation of fibers. Collectively, these results allow us to surmise a mechanism of action of MB that blocks the PrP conversion process.

2. Materials and methods

2.1. Materials

MB and Thioflavin T (ThT), at a purity ≥95%, were purchased from Sigma Aldrich. MB was dissolved in the same buffer used for the protein, depending on the experiments (see below). The stock solutions were filtered with a 0.2-mm filter, kept at 4 °C and made freshly for each independent experiment.

2.2. Monomeric and oligomeric protein production

The full-length PrP from sheep OvPrP (A^{136} R^{154} Q^{171} variant), the truncated form ΔOvPrP (103–234), the full-length mouse PrP (MoPrP) and the full-length human PrP (HuPrP) were expressed in *Escherichia coli* and purified as previously described [20]. All the mutants from sheep, OvPrP_H190A, OvPrP_H190KI208M were obtained by introducing the respective mutations into the ARQ gene cloned in a pET22bC vector by using the QuickChange mutagenesis kit (Stratagene, La Jolla, CA).

Different buffers were used to desalt the protein on a HiPrep desalting column using an AKTA FPLC chromatography equipment (GE Healthcare): sodium citrate 20 mM, pH 3.4; sodium acetate 20 mM, pH 4.6; MOPS 20 mM, pH 7.0. Final protein concentration was measured by optical density at 280 nm using an extinction coefficient of 58718 M^{-1} cm^2 for wt-OvPrP, wt-MoPrP and wt-HuPrP and all the mutants and an extinction coefficient of 18005 M^{-1} cm^2 for ΔOvPrP, deduced from the amino acid sequence.

2.3. Size exclusion chromatography (SEC)

The oligomerization pathway of the mutant OvPrP_ H190KI208M was analyzed by SEC using a TSK 4000SW gel-filtration column (60 × 0.78 cm), in sodium citrate 20 mM, pH 3.4, at 20 °C. Several PrP solutions, at the same concentration, 40 μM, were heated at 50 °C for incubation times ranging from 0 to 90 min, in a Perkin Elmer GenAmp2400 thermocycler.

The formation of the O1 and O3 oligomers was obtained by heating a solution of wt-OvPrP and wt-MoPrP (100 μM), in sodium citrate 20 mM pH 3.4, at 60 °C for 12 h and 50 °C for 8 min, respectively. Homogeneous fractions of each oligomer were collected.

2.4. Static light-scattering (SLS)

SLS kinetics experiments were performed on a homemade device with four lasers (407, 473, 533, and 633 nm) using a 2 mm cuvette. The oligomerization of wt-OvPrP, wt-MoPrP and the mutants OvPrP_H190A and OvPrP_H190KI208M was monitored in the absence and presence of MB at 50 °C and in sodium citrate 20 mM, pH 3.4 or MOPS 20 mM, pH 7.0. The concentration of protein samples was in the range 30–50 μM, and several PrP:MB molar ratios were analyzed. To estimate the percentage decrease of the SLS intensity in the presence of MB with respect to that one without MB, the SLS values, after 60 min, were considered for each curve.

For depolymerization experiments, O1 and O3 oligomers were incubated in the SLS device in the absence and presence of MB at 75 and 55 °C, respectively. The concentration of oligomers used was 8 μM and the depolymerization was performed using a oligomer:MB molar ratio of 1:4. Signal processing was achieved by a homemade MatLab program.

2.5. Differential scanning calorimetry (DSC)

DSC thermograms were obtained by a MicroCal DSC instrument with cell volumes of 0.5 mL, at a scan rate of 60 and 90 °C/h. All the experiments were performed with full-length wt-OvPrP at 50 μM, using three different pH conditions: sodium citrate 20 mM, pH 3.4; sodium acetate 15 mM, pH 4.6 and MOPS 20 mM, pH 7.0. For each condition, at least two thermograms were recorded with and without MB, at PrP:MB molar ratio of 1:4. DSC thermograms were analyzed with ORIGINLab software. Deconvolution of DSC curves obtained at pH 7.0 was achieved by a homemade MatLab program applying the Lumry–Eyring model for irreversible processes [21]. To estimate the percentage of oligomers formed in the absence and presence of MB, we calculated the area of the deconvoluted peaks corresponding to the second transition.

2.6. Nuclear magnetic resonance (NMR)

MB titrations were followed by recording ^{1}H-^{15}N HSQC NMR spectra of 0.2 mM samples of the ^{15}N-labeled ΔOvPrP in sodium acetate 20 mM, pH 4.6 and MOPS 5 mM, pH 7.0, at 25 °C on a Varian 600 MHz spectrometer. The water signal was suppressed by the WATERGATE pulse sequence. Additions of MB from a stock solution were done to reach the final PrP:MB molar ratios of 1:1, 1:2, 1:5 and 1:10.

2.7. PrP fibrillization and transmission electron microscopy (TEM)

The kinetics of fibril formation was monitored using a ThT-binding assay. Solvents and solutions were filtered using 0.02-μm filters prior usage. Lyophilized wt-HuPrP and wt-OvPrP were dissolved in MES 50 mM, pH 6.0. MB was dissolved in water to a final concentration of 22–220 μM. The fibrillization reaction was started diluting the PrP stock solution to a final concentration of 22 μM in GdnHCl 2.0 M and MES 0.5 mM, pH 6.0. A control sample without MB and several samples, at different PrP:MB molar ratios, were prepared and immediately incubated at 37 °C. During incubation, aliquots of the solutions were collected at regular time intervals and diluted in sodium acetate 10 mM, pH 5.0 to a final PrP concentration of 0.3 μM. Then, ThT was added to a final concentration of 10 μM. For each sample, emission spectra were recorded using a Jasco 6200 spectrofluorimeter with a 2 mm × 10 mm optical path-length cuvette and an excitation wavelength of 445 nm. Both excitation and emission slits were 5 nm. Spectra were averaged and the fluorescence intensity at emission maximum (482 nm) was determined. To evaluate if MB could interfere with the ThT emission, fluorescence spectra of the solutions containing alternatively only ThT and both ThT and MB were recorded, at the maximum concentration used for the samples PrP-MB. The emission of ThT was the same with and without MB.

Fibril morphology was analyzed by TEM using a Zeiss EM902 (80 kV) microscope. Briefly, 10 μL of the protein samples was adsorbed onto carbon-coated Formvar grids (Agar Scientific). Then, each grid was washed three times with water, stained with 2% uranyl acetate and finally air-dried.

3. Results

3.1. MB directly interacts with the ground state of PrP

To explore the interaction of MB with the native monomeric folded PrP, we carried out NMR experiments at both pH 4.6 and 7.0. Titration of ^{15}N-labeled ΔOvPrP (ARQ variant) with MB at pH 4.6 followed by ^{15}N-HSQC spectra did not result in variations either in the chemical shifts or in the peak intensity up to a PrP:MB molar ratio of 1:10 (data not shown). This result was confirmed by DSC experiments (Supplemental Fig. S1) performed on wt-OvPrP at pH 4.6, which showed no variation of the melting temperature in the presence of MB, suggesting that MB does not have any stabilizing or destabilizing effect on the native PrP structure.

Contrarily, NMR titrations at pH 7.0 showed small but clear chemical shift perturbations of up to nine resonances, namely N146, N156, Y158, Y160, K188, T191, two of the T193-196 multi-threonine stretch, presumably T194 and T195 and Q215 (Fig. 1A). Identification of these peaks allowed us to map the interaction in a quite extended cleft on the protein surface (1024 Å^3), which would be able to host MB. The cleft is lined by about 20 residues coming from the region around the helix H1 and mainly from helix H2 and the N-terminal region of helix H3 (Fig. 1B and C). Out of nine residues with chemical shifts perturbed by the MB addition, six (N146, K188, T191, T194, T195 and Q215) fall in the cavity, and most of them are located on the C-terminal tip of H2. The remaining residues out of cavity, Y158 and Y160, lie in the loop connecting the helix H1 with the strand S2, whereas N156 is the last H1 residue. The presence within the cavity of a high number of ionizable residues (1 Arg, 2 Lys, 1 His and 5 Glu), which are able to affect the charge distribution, well explains the pH dependence of the cleft interaction with the positive MB molecule (Fig. 1B and C). The effective charge of His180 and of five Glu (approximate pKa 6 and 4, respectively) may play a key role in attracting the positive MB molecule, within the explored pH interval 4.6–7.0, being their pKa markedly influenced by the protein environment.

3.2. Methylene blue affects the kinetics of PrP oligomerization but not depolymerization

In previous works, it was shown that PrP undergoes a polymerization process upon thermal treatment, accompanied by the formation of different population of oligomers, depending on the PrP species, mutants and experimental conditions used [22–24]. In particular, at pH 3.4, wt-OvPrP was shown to oligomerize into three different oligomers, referred to as O1, O2 and O3, whereas wt-MoPrP and the variant OvPrP_H190A give rise mostly to O3 and O1 oligomer, respectively (see reaction scheme in Fig. 2A–C). In addition, we have designed and produced a new mutant, OvPrP_H190KI208M, for which the corresponding SEC profile revealed the formation of O3 and fibril-like assemblies, denoted P0 (Supplemental Fig. S2).

In order to evaluate if MB specifically interferes on a particular PrP oligomerization pathway, we monitored the polymerization kinetics of wt-OvPrP, wt-MoPrP, and the variants OvPrP_H190A and OvPrP_H190KI208M by SLS, in the presence and absence of MB, at pH 3.4.

The SLS kinetic curves of all the PrP forms tested are shown in Fig. 2A–D. In all cases, the kinetic profiles obtained in the presence of MB differed from those obtained in the absence of MB, and the higher the MB concentration was, the more the SLS intensity signal decreased.

To obtain a quantitative estimation of the effect of MB, we evaluated the SLS intensity decrease, which is indicative either of the oligomerization rate or of the decrease in the size of oligomers. The results showed that, at pH 3.4, MB decreased the signal intensity of wt-OvPrP, wt-MoPrP and OvPrP_H190A by about 10% at PrP:MB molar ratio of 1:1, and by about 15% at a molar ratio of 1:3. For the variant OvPrP_H190KI208M, the decrease of the SLS intensity signal was about 15% and 30% compared to the protein alone, at PrP:MB molar ratios of 1:1 and 1:3, respectively.

Taking into account that a direct interaction was observed by NMR at pH 7.0, SLS kinetic experiments were performed also at this pH on wt-OvPrP. Under this condition, the thermal treatment of the protein gives rise to the formation of mainly O1 and P0 fibril assemblies (see reaction scheme in Fig. 2E), as previously described [24]. Interestingly, the SLS intensity decreased by about 40%, already at PrP:MB molar ratio of 1:1, indicating a significant greater effect than at pH 3.4 (Fig. 2A). This general behavior clearly shows that MB is able to slow down the PrP oligomerization rate, at both pH 3.4 and 7.0, even though the effect is much higher in neutral conditions. All together, these experiments suggest that MB more efficiently affects the pathway of O1 and P0 assemblies which are favorized at neutral pH. To determine if the decrease of oligomer assemblies is due to their destabilization in the presence of MB, we carried out SLS depolymerization experiments on the two most representative oligomers O1 and O3, in the absence and presence of MB. The SLS iso-kinetics depolymerization curves, shown in Fig. 3, indicated that MB does not affect the stability of oligomer assemblies.

Fig. 1. Mapping the surface of interaction with MB on native folded state of PrP. (A) Overlay of ^{15}N-HSQC spectrum of ΔOvPrP (black) with spectrum of ΔOvPrP titrated with MB (magenta) at a 1:5 PrP:MB molar ratio. Assignment of the resonances that shift more than 0.03 ppm is indicated. (B) Ribbon representation of ΔOvPrP structure (pdbcode 1y2s). Binding surface cleft is shadowed. The cavity is lined by side chains of about 20 residues coming from loop S1H1 in blue (F144, N146), helix H1 in blue (E149), helix H2 in green (H180, V183, N184, V187, K188, T191, V192, T194, T195), loop H2H3 in orange (E199) and helix H3 in red (E203, I206, K207, E210, R211, E214, Q215). The nine residues underlined are ionizable. The nine residues with resonances perturbed by MB addition are drawn as stick in magenta; the remaining ones are drawn as lines in the same color of the secondary structure element to which they belong. (C) The same representation as in (B), rotated by about 90°.

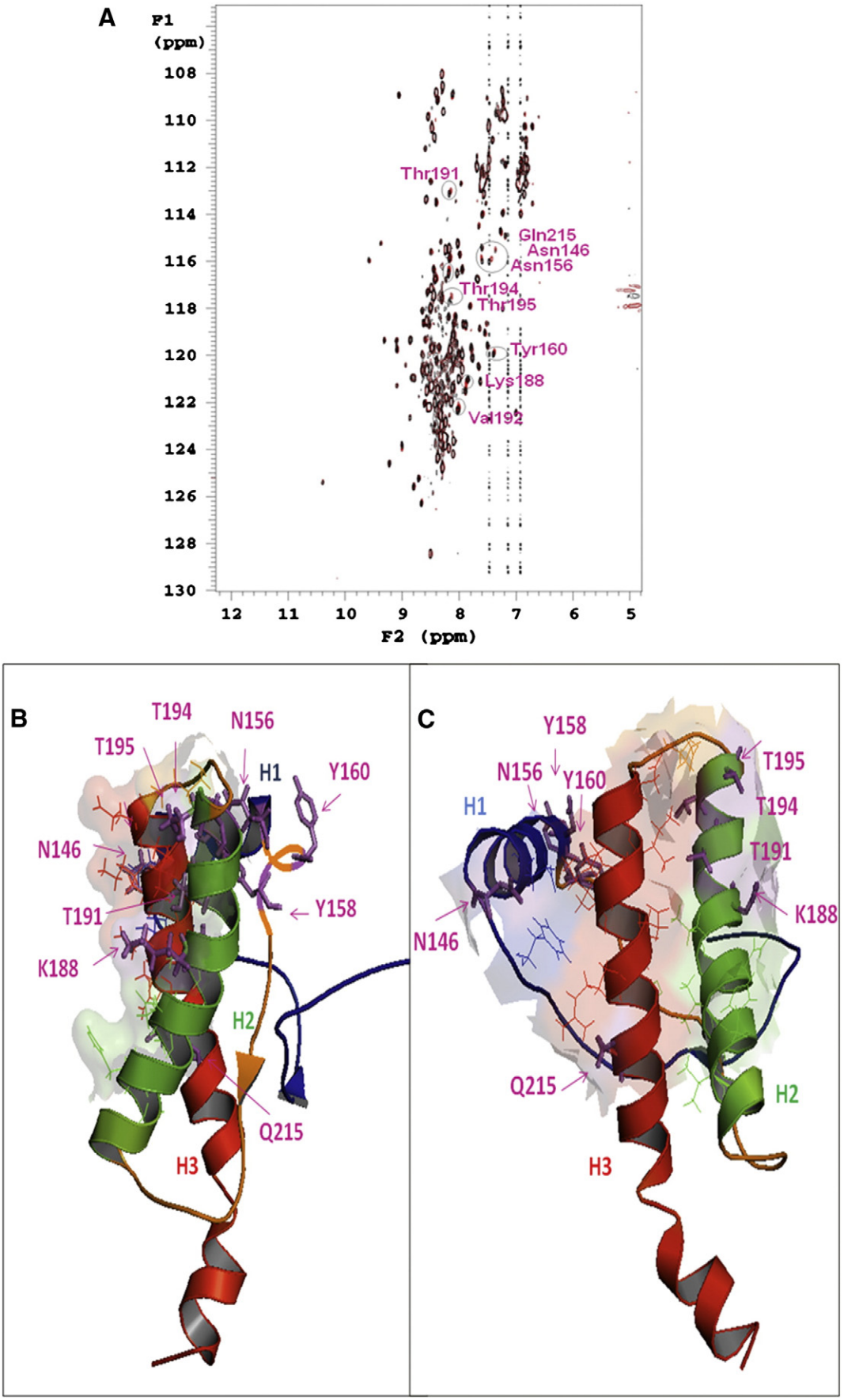
A
F1 (ppm)
108
110
112
114
116
118
120
122
124
126
128
130
12
11
10
9
8
7
6
5
F2 (ppm)
Thr191
Gln215
Asn146
Asn156
Thr194
Thr195
Tyr160
Lys188
Val192
B
T194
N156
T195
H1
Y160
N146
Y158
T191
K188
H2
Q215
H3
C
Y158
T195
N156
Y160
H1
T194
T191
K188
N146
Q215
H2
H3

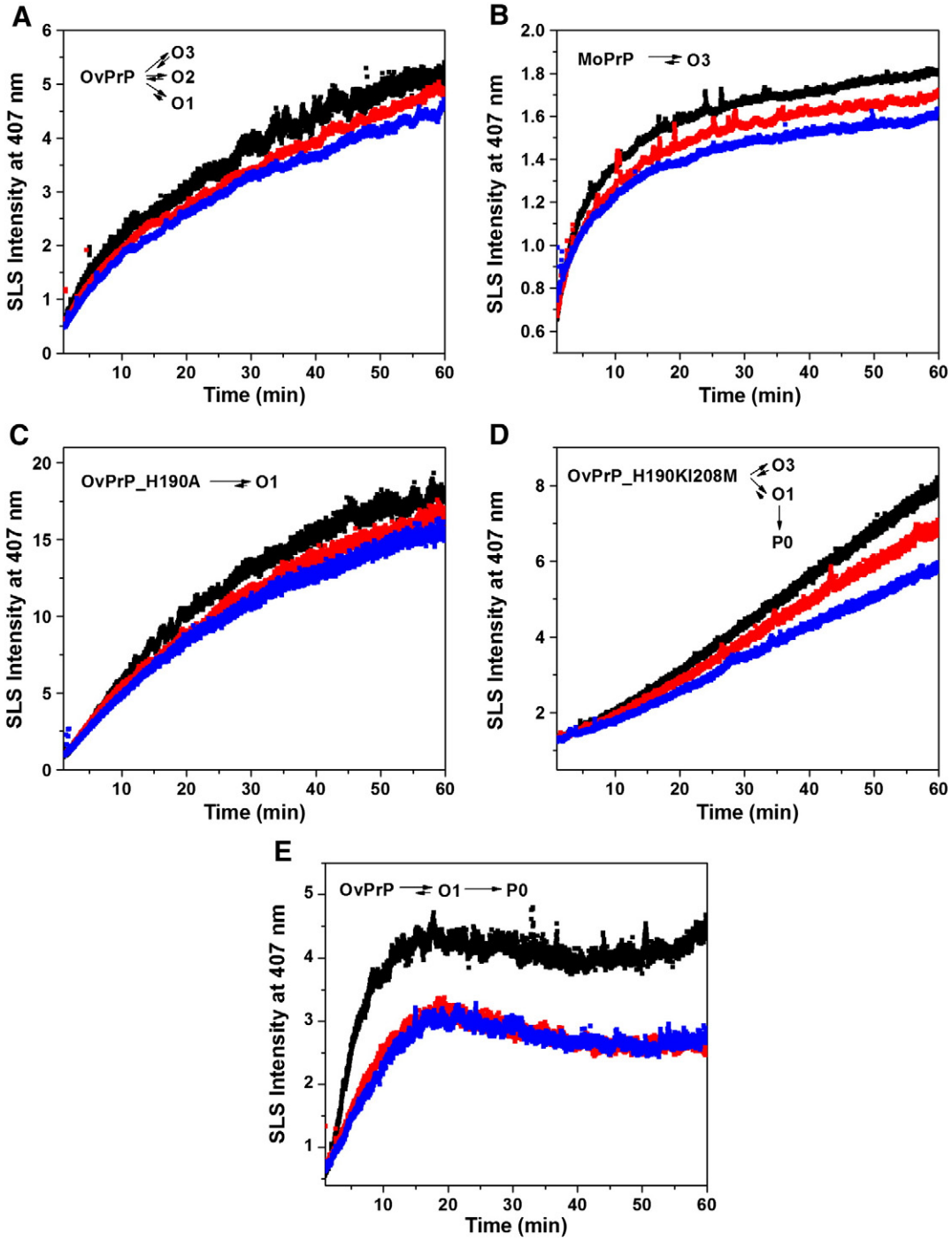

Fig. 2. Polymerization kinetics of the various PrP forms tested, in the absence and presence of MB. Time evolution SLS curves, recorded monitoring the intensity signal at 407 nm and at pH 3.4 of (A) wt-OvPrP, (B) wt-MoPrP, (C) OvPrP_H190A, (D) OvPrP_H190KI208M, and at pH 7.0 of (E) wt-OvPrP. The kinetic curves recorded in the absence of MB are depicted in black, the kinetic curves recorded at a PrP:MB molar ratio of 1:1 in red, and at PrP:MB molar ratio of 1:3 in blue. The scheme of the oligomerization reaction is also shown in each panel.

3.3. MB limits the amount of PrP oligomers

To evaluate the effects of MB on the unfolding/oligomerization process of PrP, DSC thermograms of wt-OvPrP, at pH 3.4 and 7.0, were recorded in the absence and presence of MB. The DSC thermograms, at both pH, showed two endothermic peaks corresponding to two transitions, in agreement with previous experiments [25,26]. These two transitions were explained as a PrP unfolding/oligomerization process, followed by a depolymerization process [25].

In acidic conditions, the thermograms with and without MB are very similar (Fig. 4A). The area of both peaks, as well as the transition temperatures in the two thermograms are roughly comparable, being a small area reduction detected only for the second peak, in the presence of MB. This finding indicates that, at pH 3.4, MB barely influences either the unfolding/oligomerization or the depolymerization process of PrP.

On the contrary, in neutral conditions, the thermogram of wt-OvPrP with MB is markedly different compared to the one in the absence of

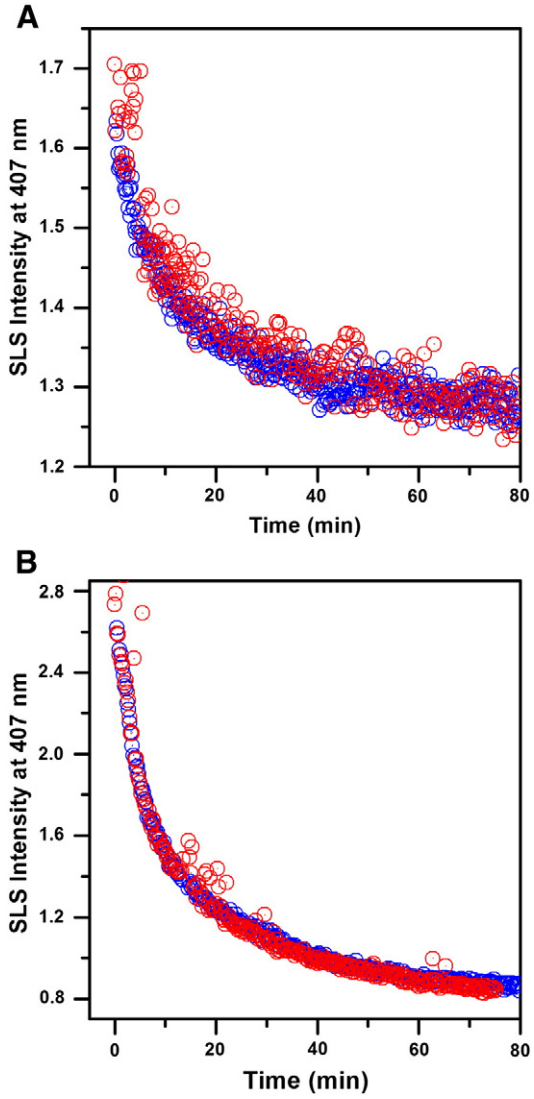

Fig. 3. Depolymerization kinetics of PrP oligomers. Time evolution SLS curves, recorded monitoring the intensity signal at 407 nm, in the absence and presence of MB, at pH 3.4 of (A) O3 and (B) O1 oligomer. The kinetic curves recorded in the absence of MB are depicted in blue, and the kinetic curves recorded at a PrP:MB molar ratio of 1:4 are in red.

MB. In particular, the area of the second peak is considerably reduced (Fig. 4B). Since this area is proportional to the relative amount of oligomers formed during the first transition, thermograms have been deconvoluted to obtain a quantitative estimation of the oligomer reduction observed in the presence of MB. As shown in Fig. 4C, deconvolution of the first peaks, obtained with and without MB, shows no significant differences. Differently, deconvolution of the second peaks, relative to the depolymerization of oligomers formed in the first transition, reveals meaningful differences in both the surface area and the transition temperature. Indeed, in the presence of MB, the peak area is reduced by about 28%, indicating a significant decrease of the oligomer formation, and the transition temperature decreased by about 4 °C, in accordance with the Lumry–Eyring model, in which the concentration of oligomers is directly proportional to the second transition temperature [21,26].

These findings fully confirm that MB significantly interferes with the PrP oligomer formation at physiologic pH, by reducing both the oligomerization rate, as observed by SLS, and the amount of oligomers formed along the oligomerization pathway.

3.4. MB completely suppresses PrP fibril formation

Finally, the action of MB on fibril formation was also studied. wt-HuPrP and wt-OvPrP fibrils were generated at pH 6.0 in the absence – as control – and in the presence of MB. The PrP fibril formation was monitored using ThT-binding assay. In Fig. 5A and B the kinetic curves of the wt-HuPrP and wt-OvPrP fibril formation are shown, at different PrP:MB molar ratios. For both PrP species, in the absence of MB, the ThT signal intensity gradually rises with a sigmoidal shape, indicating the formation of PrP fibrils. Differently, in the presence of MB, within the range 1:0<PrP:MB<1:2, a longer lag phase is observed, which increases in a dose-dependent manner (see Supplemental Fig. S3A and B) and, at PrP:MB molar ratios equal to or lesser than 1:2, the fibril formation was completely inhibited.

A valuable confirmation that the fibril formation is suppressed by MB was obtained by TEM images (Fig. 5C–F). For both wt-HuPrP and wt-OvPrP, typical fibrillar structures were observed in the absence of MB (Fig. 5C and E). On the other hand, surveying the entire EM grid, none or very little fibrillar material was observed for samples incubated with MB at PrP:MB molar ratios lesser than 1:2 (Fig. 5D and F). The TEM images of the solutions at PrP:MB molar ratios higher than 1:2 confirm the results obtained by ThT fluorescence assays, showing the formation of fibrils, even if a little decrease on the fibril amount was detected (Supplemental Fig. S3C–F).

4. Discussion

A widely explored field in prion diseases is the evaluation, primarily in vitro, of compounds that can interfere with the $PrP^{C}\rightarrow PrP^{Sc}$ conversion, and be potentially used as drugs against these diseases. Different drug discovery strategies have been reported [27–29], but for many of these compounds, the clinical potentiality is unclear, because of pharmacological hurdles. For these reasons, we sought a known molecule that could fulfill safety features required for drugs delivery to humans and animals, and could actually be considered for future *in vivo* applications. The pharmacokinetic and toxicological properties of MB are well-known. More importantly, MB has been shown to overpass the blood–brain barrier [11,12] and thus is suitable to target PrP in the brain. Previous data on the beneficial effects of MB for the treatment of neurodegeneration due to protein misfolding and aggregation [9,10] suggest a general action of MB as an anti-aggregation compound. As far as the prion is concerned, MB was already investigated a decade ago [17]. In neuroblastoma ScN2a prion infected cells, MB was shown to be cytotoxic for these cells and not to impair the PrP^{Sc} formation. Anyhow, it should be noted that its high toxicity for ScN2a cells might have not allowed to examine its effectiveness against PrP^{Sc} formation [17]. More recently, positive data were obtained about MB treated prion-filtered red cells utilized for neonatal transfusion to reduce the risk of variant Creutzfeldt–Jakob disease transmission [18]. Therefore, it would be worthwhile to conduct further studies. In this work, we provide the first clear evidence of an effect of MB on PrP oligomer and fiber formation pathways, in vitro, and a mechanism by which this occurs.

By dissecting the action of MB along each step of the PrP aggregation pathway, we demonstrated that MB (i) directly binds to a surface cleft of native PrP, (ii) significantly affects the oligomerization kinetic rate of all the PrP forms used, (iii) limits the amount of oligomers formed during the heat-induced unfolding/oligomerization process, and (iv) completely suppresses fibril formation.

Interestingly, a pH dependence of MB action, driven by the variable charge distribution of the cleft on PrP surface, was systematically observed in all NMR, SLS and DSC experiments, even though these techniques measured distinct entities, under very different conditions. At pH 3.4 and 50 °C, SLS analysis showed a lower effect of MB on PrP oligomerization process with respect to neutral pH. On the other hand, only at pH 7.0, DSC and NMR experiments showed a

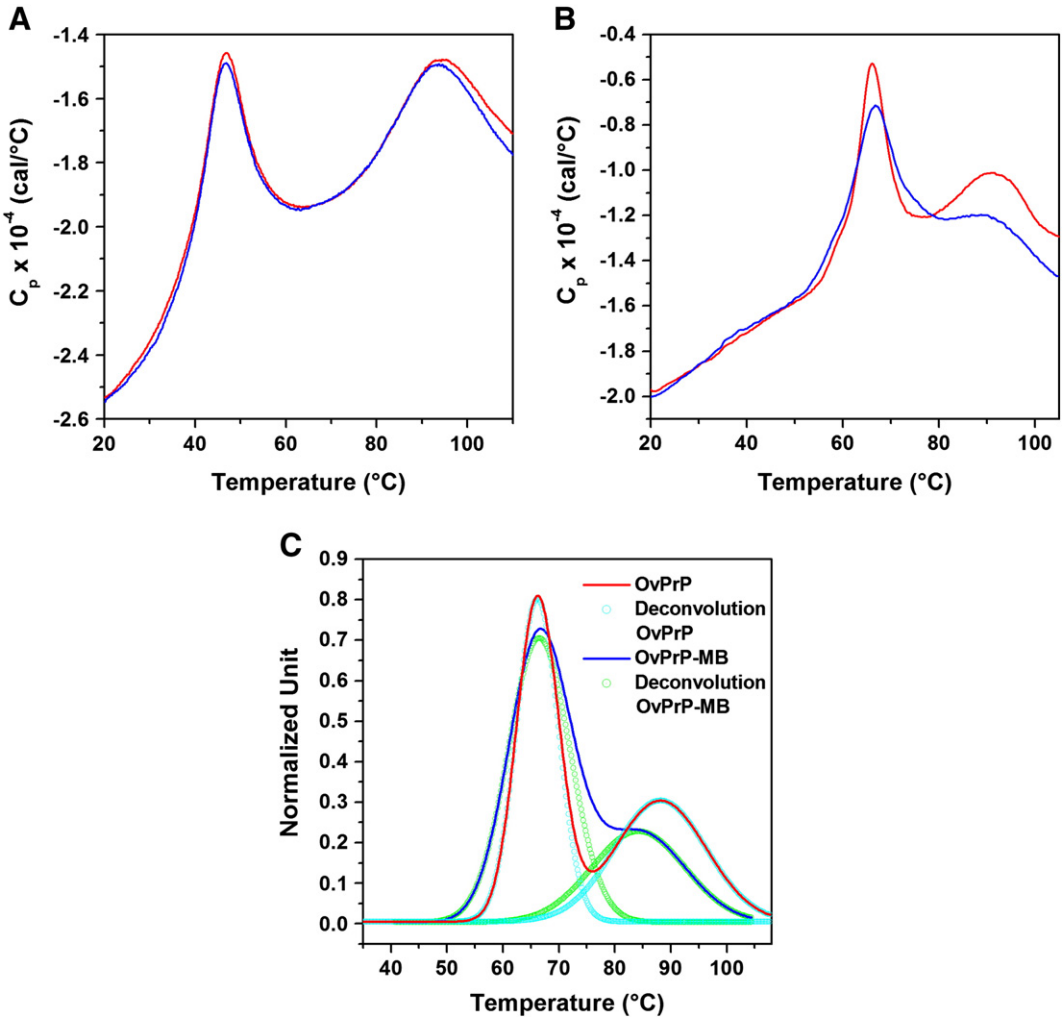

Fig. 4. DSC thermograms of wt-OvPrP, in the absence (in red) and presence (in blue) of MB, at (A) pH 3.4 and (B) pH 7.0. (C) Deconvolution of the experimental DSC curves obtained at pH 7.0. Continuous lines correspond to the experimental C_p data. Symbols represent the predicted C_p curves (in cyan without MB, in green with MB) of each transition peak in which the global curves can be deconvoluted. The PrP:MB molar ratio was 1:4.

clear influence of MB. Indeed DSC revealed a marked effect of MB on heat-induced processes. NMR titration revealed a clear chemical shift variation of 9 residues of the monomeric PrP at room temperature. The major effects were then consistently observed at physiological pH, indicating that MB is suitable to efficiently act *in vivo*. It is worth noting that a greater inhibition effect was observed for the oligomerization reaction generating fiber-like species, such as for the double mutant. This suggests that MB may have an inhibitory action directed toward fibrillization, which was confirmed by TEM experiments that clearly indicated the complete inhibition of fibril formation, below a molar ratio PrP:MB of 1:2.

Our results well agree with literature data on other amyloidogenic proteins from which it emerges that oligomerization and/or fibrillization are the steps affected by MB, even though its way of action seems very variable [13–16]. Indeed, MB may have different targets, and thus different modes of anti-aggregation action. For the $A\beta_{42}$ peptide Necula et al. [13] reported that MB inhibits the oligomerization through a stabilization of prenuclear $A\beta_{42}$ assembly. In their investigation of the effects on soluble oligomers of $A\beta_{42}$ of MB and other small aromatic molecules, Ladiwala et al. [30] highlighted their action of remodeling mature protein aggregates by converting soluble oligomers into off-pathway non toxic aggregates. Moreover, MB has been shown to block the tau–tau binding interaction, inhibiting tau filament formation in vitro, even though recent papers argue for lack of MB effect on tau aggregation *in vivo* [14,31]. MB is also able to inhibit fibril formation of TDP-43 by binding dimers and oligomers [16].

As far as PrP is concerned, it is worth underlining that our in vitro results do not contradict those obtained by Korth et al. [17], which were obtained in highly different conditions, specifically in neuroblastoma ScN2a cells infected by a given prion strain. The present study was conducted in vitro using a variety of biophysical techniques. We believe that our results can contribute to understand the action of MB on the various steps on the route toward the fiber formation.

The potential anti-prion agents hitherto evaluated act through different mechanisms. These compounds were shown to antagonize PrP conversion by a direct interaction with the native PrP [32–34] or by acting on the PrP species formed along the oligomerization/fibrillization pathway [29] or by sequestering the infectious self-propagating template PrP^{Sc} [35]. Our results clearly indicate a direct interaction between MB and the native monomeric folded PrP, at physiological pH, and rule out a direct interaction with the oligomeric PrP forms. Specifically NMR experiments showed that MB binds to an external cleft that contains residues belonging to the C-terminal tip of H2 helix (Fig. 1B). This part together with the region around helix H1 are under-protected regions, having quite a number of solvent exposed backbone H-bonds [19]. Indeed, these H-bonds are not protected against water interaction. As a result, the regions embodying such H-bonds are structurally more labile, and could act as aggregation *loci*, leading to fibrillar polymerization [19]. In this scenario, the binding of MB to the cleft of the protein may

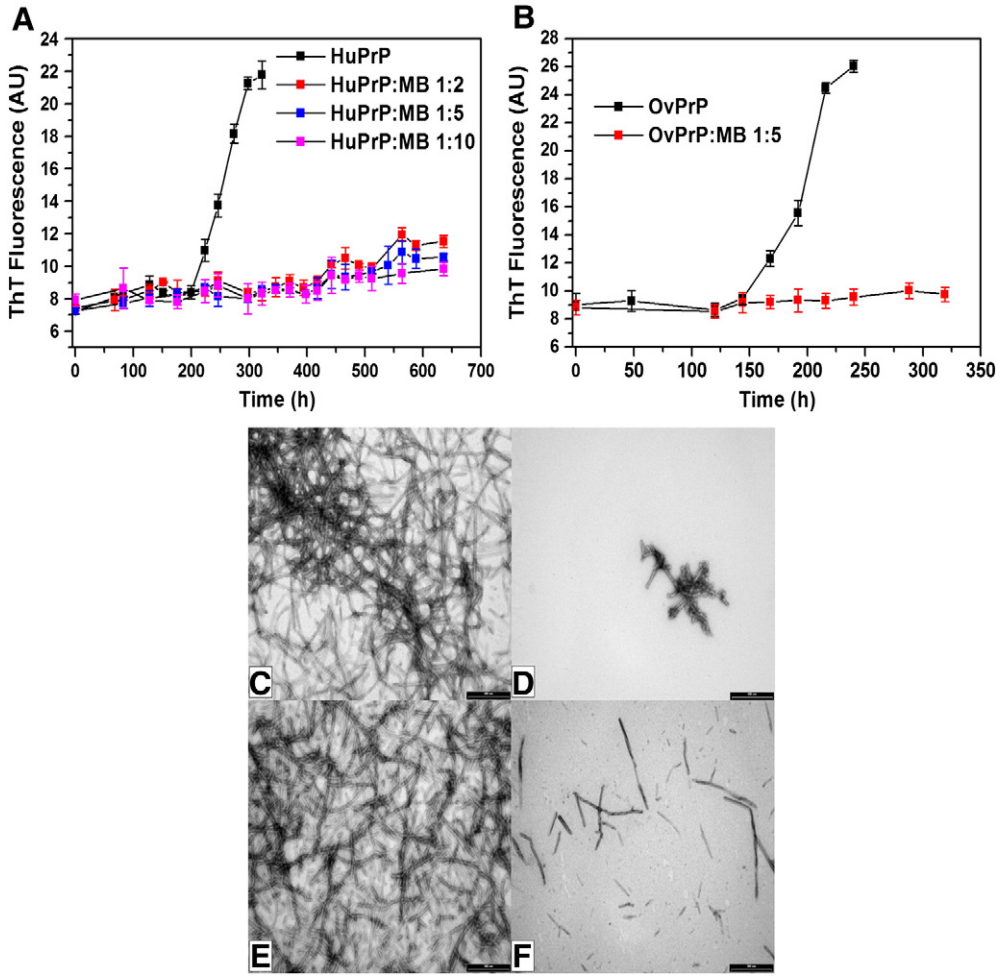

Fig. 5. Inhibition of wt-HuPrP and wt-OvPrP fibrillization mediated by MB. ThT fluorescence measurements of fibrillogenesis of (A) wt-HuPrP and (B) wt-OvPrP in the absence and presence of several concentrations of MB. Results represent means ± SD ($n = 3$). TEM images of wt-HuPrP fibrils formed (C) in the absence of MB (as control) and (D) in the presence of MB at a HuPrP:MB molar ratio of 1:5. TEM images of wt-OvPrP fibrils formed (E) in the absence of MB (as control) and (F) in the presence of MB at a OvPrP:MB molar ratio of 1:5. Scale bar: 0.5 μm.

hamper the oligomer formation and hence blocks the pathway to fiber formation. However, it is noteworthy that, although our results do not show any direct interaction with the oligomeric PrP forms, they do not rule out the hypothesis of an inference of MB on early intermediates that precede the formation of oligomers.

To sum up, our work is the first that shows the great potentiality of MB as an anti-aggregation compound for prion conversion. The cleft exposed to the solvent (Fig. 1B and C) that we find hosting MB embodies the C-terminal tip of H2 helix, a known structurally instable PrP region that may favor partially unfolded structures with a resulting potential for aggregation [19]. A drug such as MB, which well fits into the cavity, may then behave as an efficient obstacle to aggregation. In particular, the effectiveness of MB is endorsed in physiological conditions, antagonizing both oligomerization and fibrillization processes. This is a highly valuable feature of MB because it interferes with both PrP forms carrying the toxicity and infectivity in prion diseases. Indeed, either soluble oligomers or insoluble fibrils were reported to be neurotoxic in vitro and *in vivo* [36,37], whereas PrP fibrils were also shown to be infectious *in vivo* [38]. In conclusion, these results pave the way to the evaluation of MB in *in vivo* studies and preclinical testing for prion diseases.

Acknowledgements

Financial support for this work was provided by the PRIN 2007, MIUR, Rome, by the University of Naples "Federico II", Italy and by French National Institute of Agronomic Research (INRA) including INRA-Package, Alliance Biosecure. AP and KP were supported by MRC (Grant ref. U117584256).

Appendix A. Supplementary data

Supplementary data to this article can be found online at http://dx.doi.org/10.1016/j.bbadis.2012.09.005.

References

[1] S.J. DeArmond, Alzheimer's disease and Creutzfeldt–Jakob disease: overlap of pathogenic mechanisms, Curr. Opin. Neurol. 6 (1993) 872–881.
[2] S.B. Prusiner, Shattuck lecture–neurodegenerative diseases and prions, N. Engl. J. Med. 344 (2001) 1516–1526.
[3] A. Aguzzi, C. Haass, Games played by rogue proteins in prion disorders and Alzheimer's disease, Science 302 (2003) 814–818.
[4] K.F. Winklhofer, J. Tatzelt, C. Haass, The two faces of protein misfolding: gain- and loss-offunction in neurodegenerative diseases, EMBO J. 27 (2008) 336–349.
[5] S.B. Prusiner, Prions, Proc. Natl. Acad. Sci. U. S. A. 95 (1998) 13363–13383.
[6] B. Caughey, P.T. Lansbury, Protofibrils, pores, fibrils, and neurodegeneration: separating the responsible protein aggregates from the innocent bystanders, Annu. Rev. Neurosci. 26 (2003) 267–298.
[7] H. Rezaei, Prion protein oligomerization, Curr. Alzheimer Res. 5 (2008) 572–578.
[8] J.W. Kelly, The alternative conformations of amyloidogenic proteins and their multi-step assembly pathways, Curr. Opin. Struct. Biol. 8 (1998) 101–106.
[9] R.H. Schirmer, H. Adler, M. Pickhardt, E. Mandelkow, Lest we forget you—methylene blue …, Neurobiol. Aging 32 (2011) 2325.e7–2325.e16.

[10] M. Oz, D.E. Lorke, G.A. Petroianu, Methylene blue and Alzheimer's disease, Biochem. Pharmacol. 78 (2009) 927–932.
[11] J.L. O'Leary, J. Petty, A.B. Harris, J. Inukai, Supravital staining of mammalian brain with intraarterial methylene blue followed by pressurized oxygen, Stain Technol. 43 (1968) 197–201.
[12] C. Peter, D. Hongwan, A. Kupfer, B.H. Lauterburg, Pharmacokinetics and organ distribution of intravenous and oral methylene blue, Eur. J. Clin. Pharmacol. 56 (2000) 247–250.
[13] M. Necula, L. Breydo, S. Milton, R. Kayed, W.E. van der Veer, P. Tone, C.G. Glabe, Methylene blue inhibits amyloid Aβ oligomerization by promoting fibrillization, Biochemistry 46 (2007) 8850–8860.
[14] S. Taniguchi, N. Suzuki, M. Masuda, S. Hisanaga, T. Iwatsubo, M. Goedert, M. Hasegawa, Inhibition of heparin-induced tau filament formation by phenothiazines, polyphenols, and porphyrins, J. Biol. Chem. 280 (2005) 7614–7623.
[15] A.M. Wang, Y. Morishima, K.M. Clapp, H.M. Peng, W.B. Pratt, J.E. Gestwicki, Y. Osawa, A.P. Lieberman, Inhibition of hsp70 by methylene blue affects signaling protein function and ubiquitination and modulates polyglutamine protein degradation, J. Biol. Chem. 285 (2010) 15714–15723.
[16] M. Yamashita, T. Nonaka, T. Arai, F. Kametani, V.L. Buchman, N. Ninkina, S.O. Bachurin, H. Akiyama, M. Goedert, M. Hasegawa, Methylene blue and dimebon inhibit aggregation of TDP-43 in cellular models, FEBS Lett. 14 (2009) 2419–2424.
[17] C. Korth, B.C. May, F.E. Cohen, S.B. Prusiner, Acridine and phenothiazine derivatives as pharmacotherapeutics for prion disease, Proc. Natl. Acad. Sci. U. S. A. 98 (2001) 8936–8941.
[18] V.S. Hornsey, C. Casey, K. McColl, H. Young, O. Drummond, L. McMillan, A. Morrison, C.V. Prowse, Characteristics of prion-filtered red cells suspended in pathogen-inactivated plasma (MB treated or solvent-detergent treated) for neonatal exchange transfusion, Vox Sang. 101 (2010) 28–34.
[19] A. De Simone, A. Zagari, P. Derreumauxz, Structural and hydration properties of the partially unfolded states of the prion protein, Biophys. J. 93 (2007) 1284–1292.
[20] H. Rezaei, D. Marc, Y. Choiset, M. Takahashi, G. Hui Bon Hoa, T. Haertlé, J. Grosclaude, P. Debey, High yield purification and physico-chemical properties of full-length recombinant allelic variants of sheep prion protein linked to scrapie susceptibility, Eur. J. Biochem. 267 (2000) 2833–2839.
[21] J.M. Sanchez-Ruiz, Theoretical analysis of Lumry–Eyring models in differential scanning calorimetry, Biophys. J. 61 (1992) 921–935.
[22] N. Chakroun, S. Prigent, C.A. Dreiss, S. Noinville, C. Chapuis, F. Fraternali, H. Rezaei, The oligomerization properties of prion protein are restricted to the H2H3 domain, FASEB J. 24 (2010) 1–10.
[23] F. Eghiaian, T. Daubenfeld, Y. Quenet, M. van Audenhaege, A.P. Bouin, G. van der Rest, J. Grosclaude, H. Rezaei, Diversity in prion protein oligomerization pathways results from domain expansion as revealed by hydrogen/deuterium exchange and disulfide linkage, Proc. Natl. Acad. Sci. U. S. A. 104 (2007) 7414–7419.
[24] S. Prigent, H. Rezaei, PrP assemblies: spotting the responsible regions in prion propagation, Prion 5 (2011) 69–75.
[25] H. Rezaei, Y. Choiset, F. Eghiaian, E. Treguer, P. Mentre, P. Debey, J. Grosclaude, T. Haertle, Amyloidogenic unfolding intermediates differentiate sheep prion protein variants, J. Mol. Biol. 322 (2002) 799–814.
[26] H. Rezaei, F. Eghiaian, J. Perez, B. Doublet, Y. Choiset, T. Haertle, J. Grosclaude, Sequential generation of two structurally distinct ovine prion protein soluble oligomers displaying different biochemical reactivities, J. Mol. Biol. 347 (2005) 665–679.
[27] D.A. Kocisko, G.S. Baron, R. Rubenstein, J. Chen, S. Kuizon, B. Caughey, New inhibitors of scrapie-associated prion protein formation in a library of 2000 drugs and natural products, J. Virol. 77 (2003) 10288–10294.
[28] V. Perrier, A.C. Wallace, K. Kaneko, J. Safar, S.B. Prusiner, F.E. Cohen, Mimicking dominant negative inhibition of prion replication through structure-based drug design, Proc. Natl. Acad. Sci. U. S. A. 97 (2000) 6073–6078.
[29] B.E. Roberts, M.L. Duennwald, H. Wang, C. Chung, N.P. Lopreiato, E.A. Sweeny, M.N. Knight, J. Shorter, A synergistic small-molecule combination directly eradicates diverse prion strain structures, Nat. Chem. Biol. 5 (2009) 936–946.
[30] A.R. Ladiwala, J.S. Dordick, P.M. Tessier, Aromatic small molecules remodel toxic soluble oligomers of amyloid beta through three independent pathways, J. Biol. Mol. 286 (2011) 3209–3218.
[31] C.M. Wischik, P.C. Edwards, R.Y. Lai, M. Roth, C.R. Harrington, Selective inhibition of Alzheimer disease-like tau aggregation by phenothiazines, Proc. Natl. Acad. Sci. U. S. A. 93 (1996) 11213–11218.
[32] B. Caughey, R.E. Race, Potent inhibition of scrapie-associated PrP accumulation by congo red, J. Neurochem. 59 (1992) 768–771.
[33] K. Kuwata, N. Nishida, T. Matsumoto, Y.O. Kamatari, J. Hosokawa-Muto, K. Kodama, H.K. Nakamura, K. Kimura, M. Kawasaki, Y. Takakura, S. Shirabe, J. Takata, Y. Kataoka, S. Katamine, Hot spots in prion protein for pathogenic conversion, Proc. Natl. Acad. Sci. U. S. A. 104 (2007) 11921–11926.
[34] A.J. Nicoll, C.R. Trevitt, M.H. Tattum, E. Risse, E. Quarterman, A.A. Ibarra, C. Wright, G.S. Jackson, R.B. Sessions, M. Farrow, J.P. Waltho, A.R. Clarke, J. Colling, Pharmacological chaperone for the structured domain of human prion protein, Proc. Natl. Acad. Sci. U. S. A. 107 (2010) 17610–17615.
[35] S. Caspi, M. Halimi, A. Yanai, S.B. Sasson, A. Taraboulos, R. Gabizon, The anti-prion activity of Congo red. Putative mechanism, J. Biol. Chem. 273 (1998) 3484–3489.
[36] Y.J. Lee, R. Savtchenko, V.G. Ostapchenko, N. Makarava, I. Baskakov, Molecular structure of amyloid fibrils controls the relationship between fibrillar size and toxicity, PLoS One 6 (2011) e20244.
[37] M. Stefani, C.M. Dobson, Protein aggregation and aggregate toxicity: new insights into protein folding, misfolding diseases and biological evolution, J. Mol. Med. (Berl.) 81 (2003) 678–699.
[38] G. Legname, I.V. Baskakov, H.O. Nguyen, D. Riesner, F.E. Cohen, S.J. DeArmond, S.B. Prusiner, Synthetic mammalian prions, Science 305 (2004).